Electronic Supplementary Material (ESI) for Journal of Materials Chemistry B.

Supplementary Information

1. pXRD

All pXRD data were collected using a Rigaku MiniFlex II system equipped with a Co source (CoKα = 1.7899Å). Samples were analyzed from 15-80 °2θ with a 0.02° step size and a 3.0 s dwell time. A typical iron oxide pXRD pattern for a dry, magnetite sample prepared here is shown in **Figure S1**.

2. Alternating magnetic field

Composites were heated using a 6-turn, 53-mm tall solenoid supplied by a 7.5 kW AMF generator (MSI Automation, Inc.) operating at 302 kHz with an rms current of 19.8 A at maximum power. This coil, in addition to the foam sample holder used for SAR measurement, is shown in **Figure S2**.

The magnetic flux density, B, in the AMF coil was calculated from the measured potential, ε, induced in the probe-coil (an 8-turn, 1.90 mm-diameter, 5 mil tungsten wire solenoid) using **Equation S1** (all values in SI units) derived for a solenoid from Ampere's and Faraday's Law where f is the AC frequency, N_P is the number of turns in the probe coil, and A_P is the cross-sectional area of the probe coil. Mapping measurements were taken at the center and around the circumference of the 16 mm-diameter sample chamber at four planes along its 17 mm height as shown in **Figure S3**.

Equation S1

$$B_{\text{probe}} = \frac{\varepsilon_{\text{probe}}}{2\pi f N_P A_P}$$

Conversion of the magnetic flux density in gauss to the magnetic field strength, *H*, in oersted is equal to unity in a vacuum; conversion from oersted to A m^{-1} is a factor of 79.58.

3. Specific absorption rate

All SAR values reported for this study are tabulated in **Table S1** which includes the respective average film thickness and dry weight iron concentration.

A typical temperature curve used to calculate SAR is shown in **Figure S4A**. Iron-free controls were collected in the same sample chamber and coil at maximum power for a water-only trial (Figure S4B) and a dodecane-only trial (Figure S4C). These controls were subtracted from all slopes to account for the heat transferred into the coil from the induction coil for the same 5 °C temperature rise used to calculate *m* in Equation 1.

4. Nanoparticle dispersion in polymer composites

Uniformly black, dry nanoparticle composites indicated excellent particle dispersion across the surface area of all films prepared here. This observation was supported by the low error (no greater than 3.4 %) in film iron concentration measured via the phenanthroline method (see Section 2.3.3 in the main article) from coupons cut in triplicates at various locations from an approximately 10 cm by 20 cm film. Uniform film thickness was also achieved by solvent casting polymer / nanoparticle solutions on flat, poly(tetrafluoroethylene) sheets that were adhered to glass plates. This level casting procedure was performed with a 10 cm-wide casting blade which also contributed to a homogeneous particle dispersion across the film surface area.

To address nanoparticle distribution in the thickness dimension of the films, Figure S5 shows a cross-section of a typical PS film with progressive magnifications in SEM. In the bottom panel, individual particles in micron-sized aggregates are discernable; prior magnifications show that these features extend across the entire thickness of the film. This is unsurprising, as a Stokes' Law calculation for 20 nm iron oxide particles (5.1 g cm^{-3} density) settling in an 8% w/w polymer solution (1.03 g cm^{-3}, 31.8 cP (determined by falling ball viscometer)) indicate a sedimentation of approximately 1 µm during the maximum 12 hours required for film drying. With aggregation this distance would decrease, though the effective viscosity of these non-Newtonian fluids under such low strain is likely to be orders of magnitude higher, and increasing quickly as the coating dries.

5. Heat transfer modeling

All thermal models were performed in the 6.45 cm^2 by 15.2 cm long acrylic chamber shown in **Figure S6A** which also shows a cross-section of an approximately 2.5 cm-thick, PVA hydrogel in this chamber (Figure S6B). Figure S6C shows the nichrome foil heating element (2.54 cm by 7.62 cm) used to supply the temperature boundary condition for all setpoints; path resistance = 3.24 ohm.

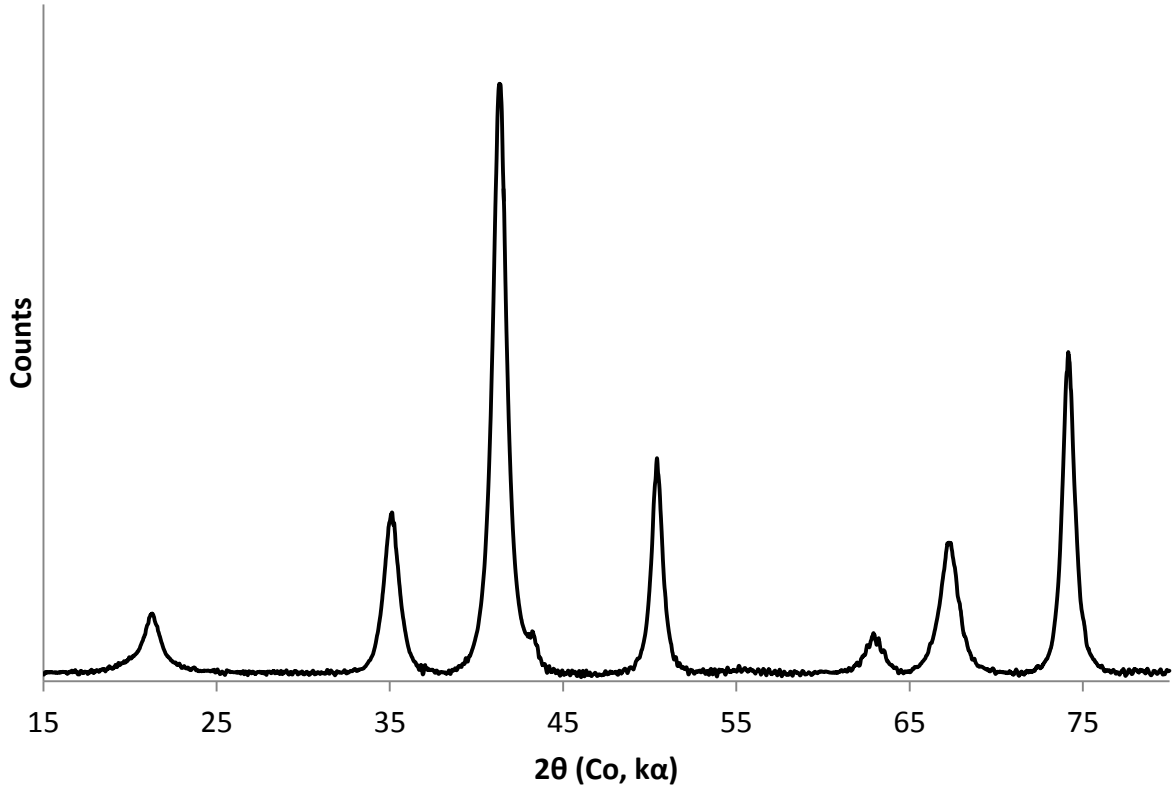

Figure S1. pXRD pattern for magnetite sample dried from suspension; unit-cell length = 8.379.

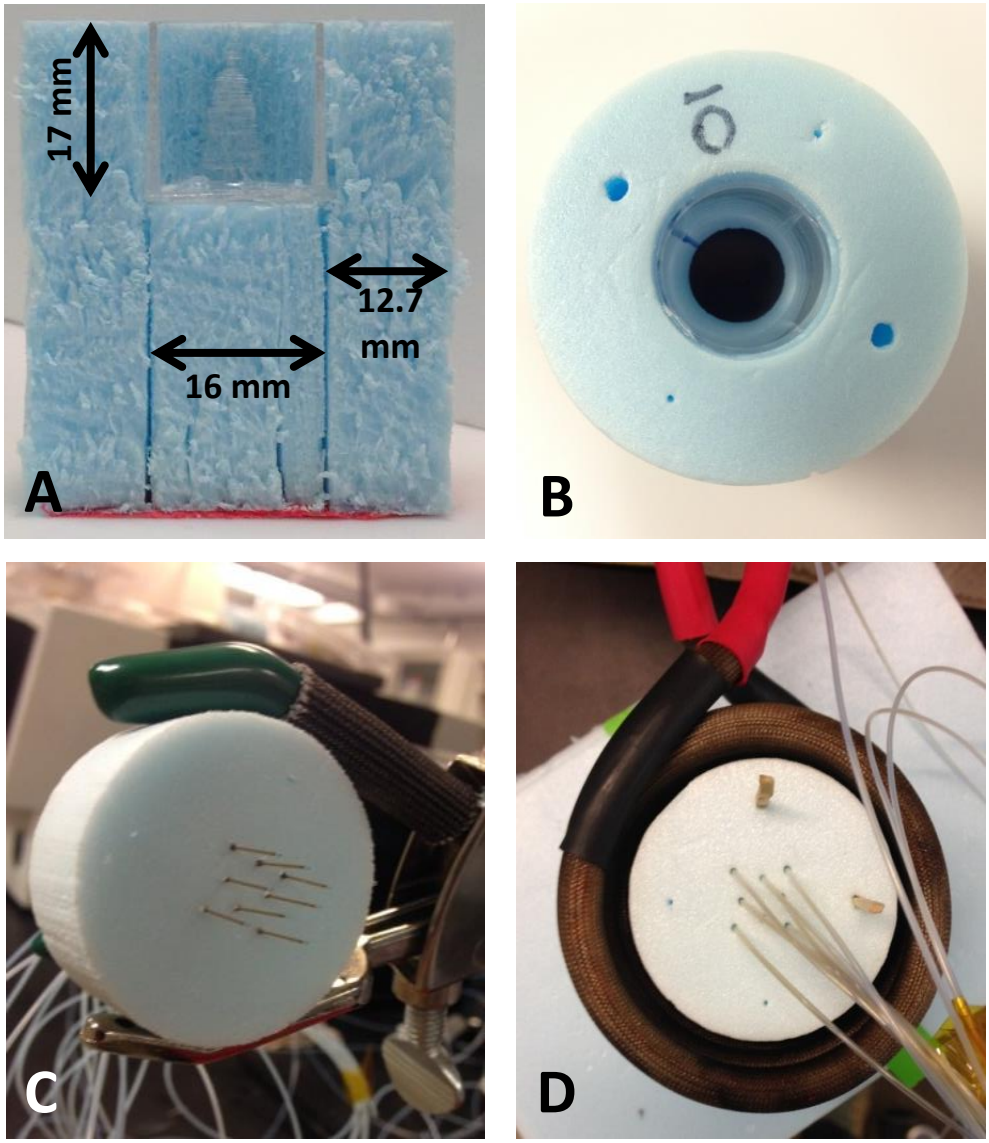

Figure S2. Cross-section of foam sample holder with polystyrene-lined sample chamber (A) top-view of sample holder/chamber with 12 mm composite coupon in the perpendicular orientation (B) sample holder lid with 8 fiber optic temperature probes (C) top-view of sample holder in 52 mm AMF coil (D).

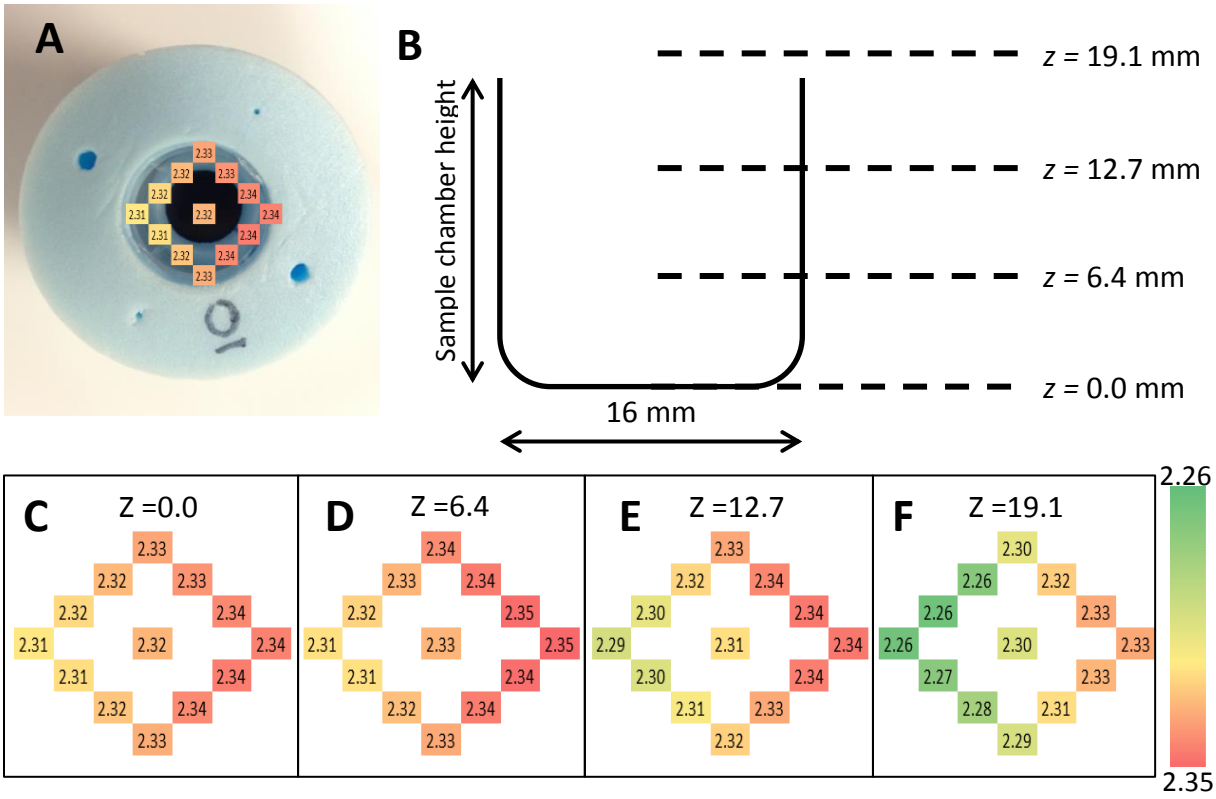

Figure S3. Alternating magnetic field mapping at four planes along the sample chamber height, *z* (depicted in panel B); values in colored boxes indicated the measured magnetic field strength, *H*, in kA m^{-1} at corresponding locations within the the sample chamber (shown in panel A) for each plane at z = 0.0 mm (C), z = 6.4 mm (D), z = 12.7 mm (E), and z = 19.1 mm (F). These values indicate a less than 1% variation in field strength throughout the entire sample chamber volume used for SAR measurements.

Table S1. Magnetite/polymer composite characteristics and corresponding SAR values; $n = 3$.

Polymer	Dry wt% Fe	Thickness (μm)	SAR (W g^{-1}) in water, ⊥ AMF	SAR (W g^{-1}) in dodecane, ⊥ AMF	SAR (W g^{-1}) in water, ∥ AMF	SAR (W g^{-1}) in dodecane, ∥ AMF
PS	8.9 ±0.1	81 ±1	289 ±29	264 ±32	489 ±43	448 ±26
PS	8.9 ±0.0	139 ±2	311 ±18	269 ±17	451 ±82	460 ±35
PS	9.3 ±0.1	182 ±0	329 ±12	293 ±15	485 ±87	420 ±30
PS	18.7 ±1.0	78 ±2	242 ±28	218 ±14	439 ±29	416 ±26
PS	19.5 ±0.1	129 ±8	261 ±14	253 ±11	488 ±23	468 ±32
PS	16.6 ±0.1	211 ±2	282 ±19	279 ±17	498 ±29	489 ±53
PS	27.4 ±0.9	68 ±3	209 ±14	193 ±35	499 ±28	451 ±41
PS	26.4 ±0.2	105 ±5	239 ±15	238 ±36	547 ±18	444 ±28
PS	26.1 ±0.0	193 ±19	250 ±10	290 ±48	562 ±37	489 ±26
PVA	17.6 ±0.6	45 ±6	322 ±30	203 ±29	626 ±37	623 ±44
PVA	17.6 ±0.1	63 ±3	329 ±18	196 ±15	636 ±51	652 ±48
PVA	17.6 ±0.1	98 ±5	361 ±15	221 ±15	717 ±33	681 ±25
PVA	28.1 ±0.2	39 ±1	359 ±28	141 ±22	666 ±53	611 ±55
PVA	27.9 ±0.1	68 ±2	308 ±29	193 ±14	633 ±26	561 ±61
PVA	28.3 ±0.4	109 ±1	336 ±19	153 ±17	637 ±29	640 ±26
PVA	39.7 ±0.1	40 ±1	188 ±18	116 ±32	656 ±37	618 ±29
PVA	40.0 ±0.2	68 ±2	207 ±12	123 ±22	574 ±36	586 ±23
PVA	40.2 ±0.5	97 ±12	330 ±50	100 ±10	574 ±46	714 ±35

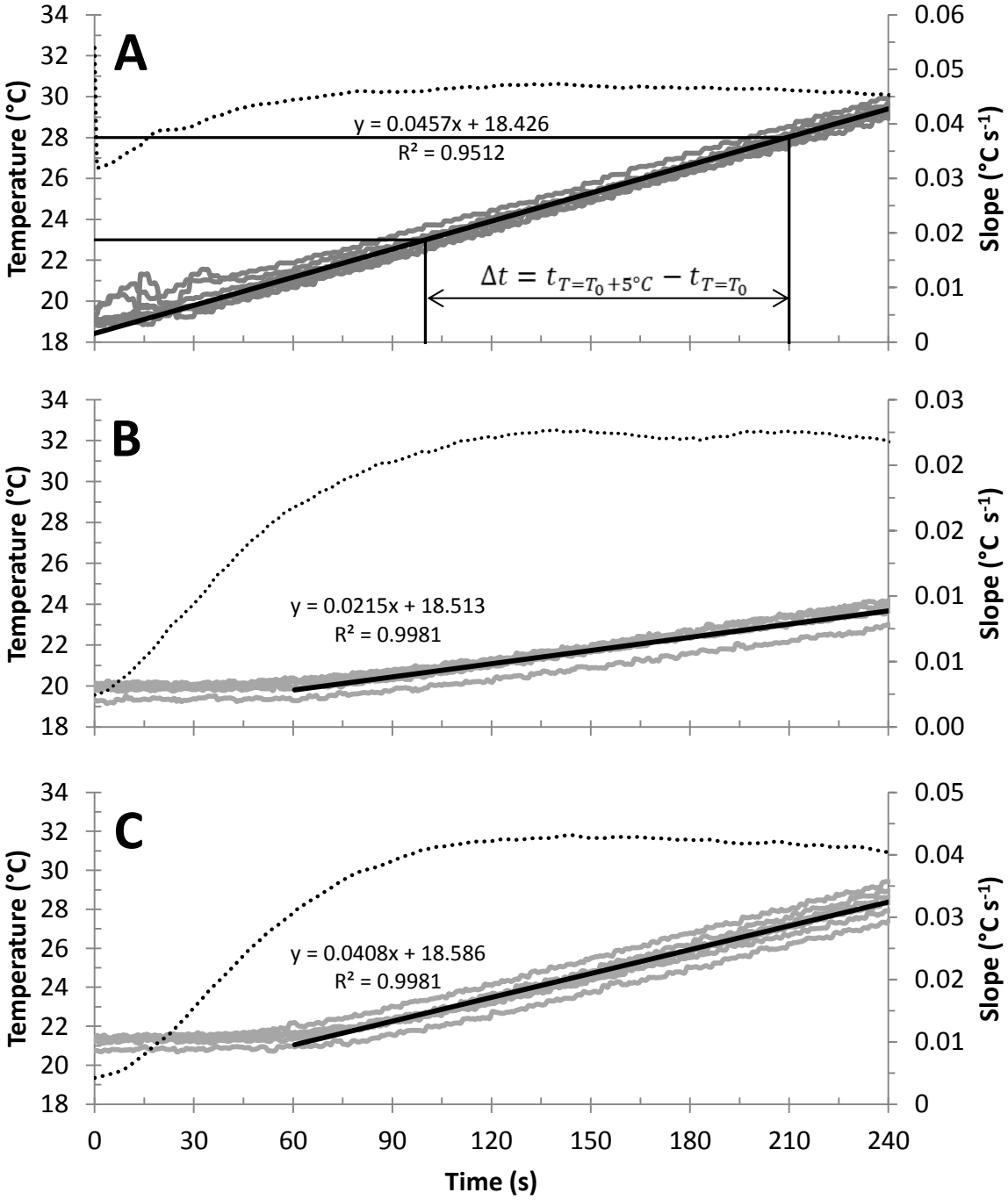

Figure S4. Transient temperature profiles in sample chamber for a 9.0wt% Fe, 81 µm-thick PS composite in water, orientated perpendicularly (A); temperature rise from induction coil in a water (B) and dodecane (C) iron-free control; grey lines indicate measurements from all 8 temperature probes (left, vertical axis); solid black line indicates linear fit to average of all temperature measurements; dotted line indicates transient slope, *m*, from Equation 1 (right vertical axis); vertical and horizontal black lines in (A) indicate Δt used in calculating SAR that corresponds to a 5 °C temperature rise.

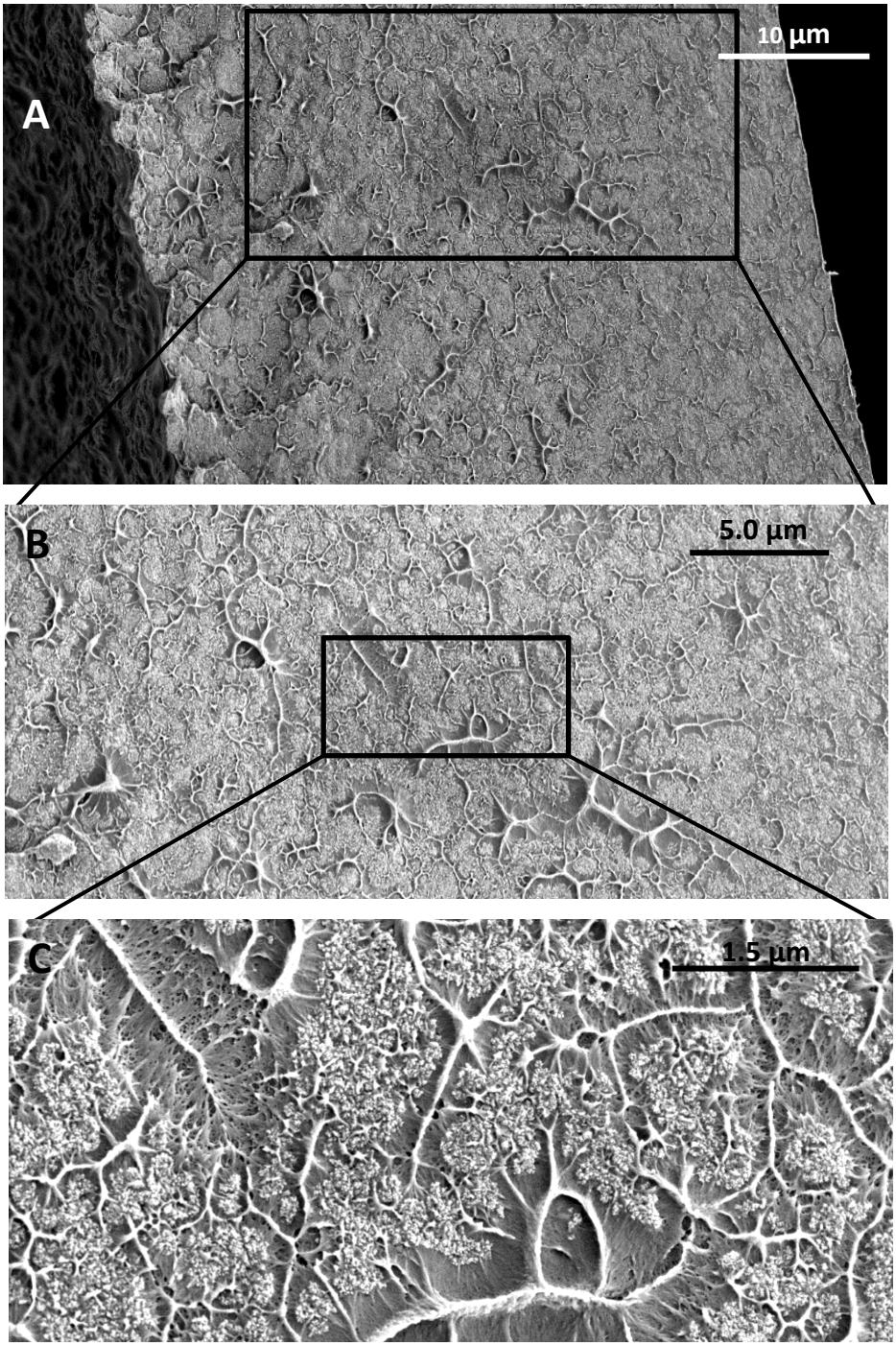

Figure S5. SEM images of a 26.1 %Fe, 193 ±19 µm-thick PS composite at three magnifications. Shown in (C) are evenly dispersed aggregates of iron oxide nanoparticles; at lower magnifaction this dispersion is retained in (B) and across the entire film thickness as shown in (A). Additionally, (A) demonstrates the presence of particle aggregates at the top corner (defined as the air side of the film after it was cast and dried) of the film composite.

Figure S6. Acrylic chamber used for thermal model (A) 6.45 cm^2 cross-section of PVA hydrogel tissue mimic (B) 19.3 cm^2-area, 25 µm-thick, nichrome foil heating element (C).